A simulation model for the density of states and for incomplete ionization in crystalline silicon. II. Investigation of Si:As and Si:B and usage in device simulation

P. P. Altermatt[a)]
Department of Solar Energy, Institute of Solid-State Physics, University of Hannover, Appelstrasse 2, 30167 Hannover, Germany

A. Schenk
ETH Zurich, Integrated Systems Laboratory, Gloriastrasse 35, 8092 Zurich, Switzerland and Synopsys Switzerland LLC Affolternstrasse 52, CH-8050 Zürich, Switzerland

B. Schmithüsen
ETH Zurich, Integrated Systems Laboratory, Gloriastrasse 35, 8092 Zurich, Switzerland

G. Heiser
School of Computer Science and Engineering, University of New South Wales, Sydney, New South Wales 2052, Australia

Building on Part I of this paper [Altermatt *et al.*, J. Appl. Phys. **100**, 113714 (2006)], the parametrization of the density of states and of incomplete ionization (ii) is extended to arsenic- and boron-doped crystalline silicon. The amount of ii is significantly larger in Si:As than in Si:P. Boron and phosphorus cause a similar amount of ii although the boron energy level has a distinctly different behavior as a function of dopant density than the phosphorus level. This is so because the boron ground state is fourfold degenerate, while the phosphorus ground state is twofold degenerate. Finally, equations of ii are derived that are suitable for implementation in device simulators. Simulations demonstrate that ii increases the current gain of bipolar transistors by up to 25% and that it decreases the open-circuit voltage of thin-film solar cells by up to 10 mV. The simulation model therefore improves the predictive capabilities of device modeling of *p-n*-junction devices. © 2006 American Institute of Physics. [DOI: 10.1063/1.2386935]

I. INTRODUCTION

In a preceding article (Part I), we collected a thorough physical understanding of the density of states (DOS) near the conduction band edge of crystalline silicon doped with phosphorus. Based on this, the DOS was parametrized with parameters derived from experiments. We approximated the DOS of the dopant band with the Gaussian function,

$$D_{\text{dop}}(E, N_{\text{dop}}) = \frac{N_{\text{dop}} b}{\sqrt{2\pi}\delta} \exp\left[\frac{-(E - E_{\text{dop}})^2}{2\delta^2}\right]. \tag{1}$$

Here, δ is the half-width of the dopant DOS, b is the fraction of carriers in localized states, and the energy of the dopant level E_{dop} is defined as the energy where the dopant DOS peaks. We expressed E_{dop} as follows:

$$E_{\text{dop}} = \frac{E_{\text{dop},0}}{1 + (N_{\text{dop}}/N_{\text{ref}})^c}, \tag{2}$$

where $E_{\text{dop},0}$ denotes the dopant energy at low N_{dop}. For an expression of δ, we chose

$$\delta = r N_{\text{dop}}^{1/2} (1 - e^{-s/N_{\text{dop}}}), \tag{3}$$

and for b we used

$$b = \frac{1}{1 + (N_{\text{dop}}/N_b)^d}. \tag{4}$$

These equations and the parameters listed in Table I reproduce measurements of incomplete ionization (ii) in Si:P in the temperature range between 300 and 30 K.

In this paper, the parametrization is extended to arsenic and boron, and the equations for ii that are suitable for implementation into device simulators are derived. Simulations demonstrate that the current gain of bipolar transistors is significantly influenced by ii.

TABLE I. The parameters used in Eqs. (1)–(4) to describe the density of states of the dopant band.

Parameter	Si:P	Si:As	Si:B
$E_{\text{dop},0}$ (meV)	45.5	53.7	44.39
N_{ref} (cm^{-3})	3×10^{18}	4×10^{18}	1.7×10^{18}
c	2	1.5	1.4
r (eV cm$^{-3/2}$)	4.2×10^{-12}	4.2×10^{-12}	4.2×10^{-12}
s (cm^{-3})	10^{19}	10^{19}	10^{19}
N_b (cm^{-3})	6×10^{18}	1.4×10^{19}	6×10^{18}
d	2.3	3	2.4
g[a]	1/2	1/2	1/4

[a]Equation (11) in Part I.

a)Electronic mail: altermatt@solar.uni-hannover.de

TABLE II. The energy of the dopant ground state at low N_{dop} and the critical N_{dop} where the *M-I* transition occurs, given for various dopants in Si. NA stands for "not available."

Material	$E_{dop,0}$ (meV)	N_{crit} (cm^{-3})
Si:Li	33.02[a]	N/A
Si:Sb	42.7[b]	3.0×10^{18b}
Si:P	45.5[a]	3.74×10^{18c}
Si:As	53.7[d]	8.5×10^{18e}
Si:Bi	71.0[f]	1.8×10^{19d}
Si:B	44.39[g]	4.06×10^{18h}
Si:Al	69.0[g]	NA
Si:Ga	72.73[g]	NA
Si:In	155.58[g]	NA

[a]Reference 2.
[b]Reference 6.
[c]Reference 5.
[d]Reference 1.
[e]Reference 7.
[f]Reference 4.
[g]Reference 8.
[h]Reference 9.

II. ARSENIC-DOPED SILICON

From Table II it follows that the donor state of As is situated deeper in the band gap[1] than the donor state of P,[2,3] and the Mott transition occurs at higher N_{dop} in Si:As (Ref. 4) than in Si:P.[5] Hence, we expect that the amount of ii is larger in Si:As than in Si:P.

In a previous paper (Part I), the amount of ii was derived from the ratio between the mobility μ_{cond} measured via conductivity and the mobility μ_H measured with the Hall effect. This ratio reflects incomplete ionization only if μ_{cond} is measured with the common assumption that $n=N_{dop}$ and if μ_H is obtained with an appropriate Hall correction factor r. The same is done here for the case of Si:As. We assume that r is identical in Si:As and in Si:P, given by Eq. (12) of Part I. This means that the scattering of free electrons at the donor ions is independent of the dopant type as will be justified below. Figure 1 shows the amount of ii in Si:As obtained with this procedure (filled symbols) in comparison with Si:P (crosses, taken from Fig. 5 of Part I). Although the data scatter considerably, it is obvious that the amount of ii is significantly larger in Si:As than in Si:P, as expected from the differences in $E_{dop,0}$ and N_{crit} between the two materials.

In order to calculate incomplete ionization in Si:As, some model parameters need to be adjusted to measurements. We do not know published measurements of the activation energy E_{act} and E_{dop} in Si:As except in boron-compensated material[13,14] or a paper[11] where E_{act} was given with rather low precision. Therefore, we assume that E_{dop} of Si:As behaves similarly to Si:P (as a function of N_{dop}), but is shifted towards higher N_{dop} (or higher energy) by the same amount as N_{crit} (or $E_{dop,0}$) differs between the two. The resulting parameters are listed in Table I. Because the experimental data scatter considerably, we did not attempt to fit the calculations with a least-square method.

In Part I, the dopant band width δ was adjusted with photoluminescence (PL) measurements. In Si:As, we know only of very few PL measurements,[15] and we are unable to
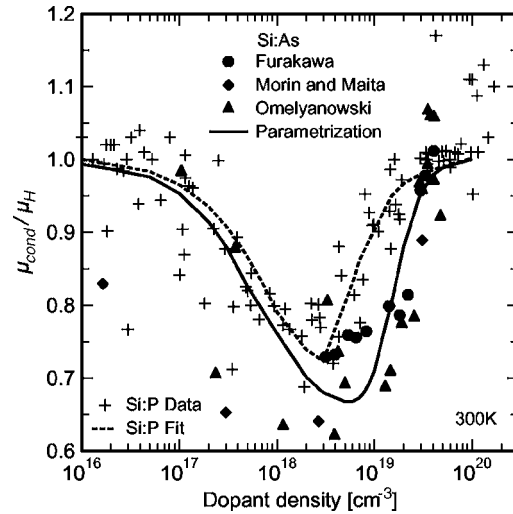

FIG. 1. The fraction between the measured conductivity mobility and Hall mobility in arsenic-doped silicon (symbols) (Refs. 10–12) reflecting an incomplete ionization (ii). Within the scatter of the data, there are significant deviations from phosphorus-doped Si (crosses, from Fig. 5. of Part I). The parametrization of ii in Si:As (solid line) and Si:P (dashed line) differs significantly as well.

derive δ as a function of N_{dop} from them. These PL spectra are similar as in Si:P,[15] indicating that δ is not vastly different between the two materials. Because δ has only a minor effect on the amount of ii (as shown in Part I), we choose the same parametrization for δ as in Si:P without causing substantial errors.

In contrast to δ, b influences the amount of incomplete ionization strongly above N_{crit}. As in Part I, b is adjusted by fitting the measurements in Fig. 1 with Eqs. (10) and (11) of Part I. The results are shown as a solid curve in Fig. 1, and the parameters for b are listed in Table I. The resulting b is different from Si:P, which is expected from the conductivity[16] and magnetoresistance[17] measurements.

Some data points at $N_{dop} < 10^{18}$ cm^{-3} in Fig. 1 show a far larger amount of ii than our calculations do. We judge these data as unprecise because we would obtain such a large amount of ii only if using a considerably larger $E_{dop,0}$ than is experimentally confirmed.[1]

As promised above, we justify in the following why we use the same Hall correction factor r in both materials. It has been concluded from a recent debate[18,19] that state-of-the-art theories predict no significant difference between electron scattering at As and at P ions.[12] Indeed, it is shown in a separate paper[20] that the measured mobility is the same in both materials if the differences in ii are included. This implies that the scattering mechanisms are the same, and so is r. Past mobility measurements indicated differences in mobility between the two materials,[21–24] because the mobility data of both materials were plotted with inconsistent assumptions, and ii was quantified insufficiently.[20]

III. BORON-DOPED SILICON

In Fig. 2, E_{act} measurements[11,13,25,26] of Si:B are compared to Si:P (the latter are taken from Fig. 3 of Part I). These data indicate differences between B and P at medium dopant densities (between 10^{17} and 10^{18} cm^{-3}). At first
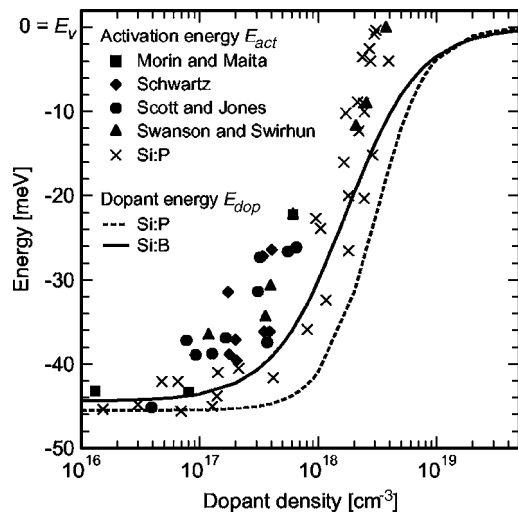
FIG. 2. Measured activation energy E_{act} in boron-doped Si (filled symbols), (Refs. 11, 13, 25, and 26) compared to Si:P (crosses, from Fig. 3. of Part I). The dopant energy E_{dop} differs from E_{act} by half the dopant band width δ. Within the scatter of the data, significant deviations are observed between the two dopant types.

glance, this may be surprising because both dopant types have practically the same $E_{dop,0}$ and N_{crit} (see Table II). The differences in E_{act} indicate that the cluster formation is different in the two materials. We conclude that this may affect E_{act} at medium N_{dop}, and that E_{dop} follows a shallower curve in Si:B than in Si:P. We parameterize E_{dop} in the following way. With the approximation that the width δ of the dopant band is the same for B and for P, the measured differences in E_{act} between the two dopant types are identical to their differences in E_{dop}, i.e., there holds $E_{dop,B} = E_{dop,P} - (E_{act,P} - E_{act,B})$. The results are shown as dashed and solid lines in Fig. 2 and were made using Eq. (2) and the parameters of Table I.

Figure 3 shows measurements of ii in Si:B (filled symbols). They were obtained with the same method as in Part I,
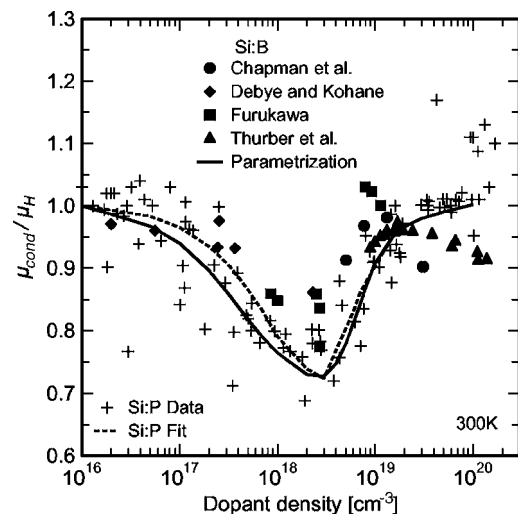

FIG. 3. The fraction between the measured conductivity mobility and Hall mobility in boron-doped Si (filled symbols) (Refs. 10–12) reflecting an ii. Within the scatter of the data, no significant deviations are observed from phosphorus-doped Si (crosses, from Fig. 5 of Part I). The parametrization of ii in Si:B (solid line) and Si:P (dashed line) differs very little as well.

except that the Hall correction factor $r = 0.8$ was taken independently of N_{dop} as previously observed.[27] At first, it is surprising that these data coincide (within their uncertainty) with the ii data of Si:P (crosses), although E_{dop} differs between boron and phosphorus. The reason for this becomes obvious by calculating ii with Eqs. (1)–(4) as well as with Eqs. (10) and (11) of Part I. The result is shown as solid line in Fig. 3 and is similar in both materials because the boron ground state is fourfold degenerate[28] (apart from a negligibly small splitting[29] of the energy level), in contrast to the phosphorus ground state whose degeneracy is only twofold.[30,31] Therefore, $g = 1/4$ for boron as has been used in previous calculations.[32,33] We like to mention that Thurber *et al.* measured a significant amount of ii at high N_{dop} (triangles in Fig. 3) because not all boron atoms were electronically active in their highly doped samples.

We assume that the broadening of the dopant band is identical in Si:B and in Si:P because we are unable to deduce E_{dop}, E_{act}, and δ independently from photoluminescence data[15,34] due to lack of data. We did not succeed in extracting the DOS from tunneling experiments[35,36] either. However, our approximation is well justified with the outcome: the resulting incomplete ionization, shown as solid line in Fig. 3, reproduces the measurements within their precision.

IV. COMPENSATION AND OTHER DOPANTS THAN P, AS, AND B

We aim that the parameters of the simulation model are deduced from measurements, such as the conductivity, the Hall mobility and, if possible, E_{act}, and other quantities. Unfortunately, we have not found sufficient experimental data in the literature on silicon doped with antimony,[10,13,21,37–44] bismuth,[1,39,45] aluminium,[10,13,39,46,47] gallium,[10,13,37–39,48,49] or indium[37,48,50] to serve as a firm experimental base for the simulation model. We therefore do not give a parametrization for these dopant types here.

Many properties of the dopant band depend on the screening among the free carriers which, in turn, depends on both the doping conditions and the injection conditions of free carriers.

Compensational doping changes the screening properties in the following way. For example, in Si:P, screening is dominated by scattering of electrons among themselves and with the P ions; when Si:P is compensated with B, electron-hole scattering comes into play, as well as scattering at B ions. The effects on the dopant band have been predicted in theoretical investigations,[51,52] showing that some phenomena are hardly affected by compensation (for example, the electronic specific heat), while others are more affected (for example, N_{crit} and E_{dop}) or even substantially affected (such as the conductivity near 0 K).[53–58]

The amount of screening can be influenced in other ways than by compensational doping. Firstly, when free carriers are additionally injected by an amount comparable to or exceeding N_{dop}, as it happens in strongly forward-biased *p-n* junctions of bipolar and power devices. Such high-injection conditions lower E_{dop}. Secondly, the depletion of carriers in *p-n* junctions results in a loss of screening because the free
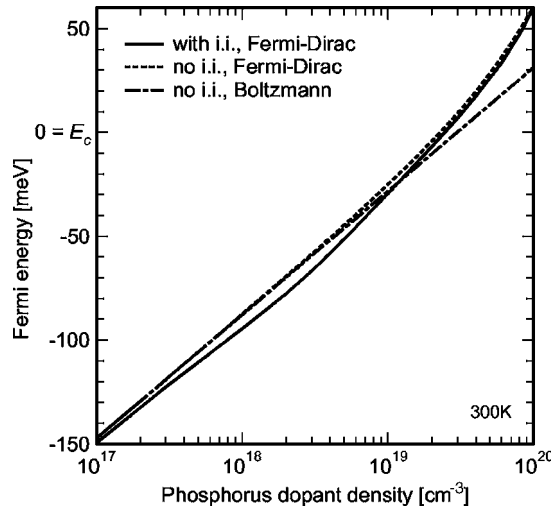
FIG. 4. The Fermi level as a function of phosphorus dopant density in thermal equilibrium, calculated with Fermi-Dirac statistics and taking incomplete ionization into account (solid line), or neglecting ii (dashed line). Calculations with Boltzmann statistics, neglecting ii are also shown for comparison (dotted line).

carrier density is normally orders of magnitude lower than the doping density. This increases E_{dop} towards $E_{dop,0}$ in depletion zones.

V. IMPLEMENTATION OF THE DOS MODEL

Equation (1)–(4) are generally unsuitable for implementation in a device simulator. A modification of the equations is needed, and we suggest the following approach.

It was demonstrated in Part I that the half-width of the dopant band, δ, has a negligible influence on the amount of ii below N_{crit} and plays a minor role above N_{crit}, where the influence of factor b dominates. Therefore, ii is implemented in the following with a discrete dopant level instead of a dopant band. This means that the Gaussian (1) is replaced by a delta function. This approximation requires only minor adjustments to b above N_{crit}. The equations for the degree of ionization, Eqs. (10) and (11) in Part I, then become

$$\frac{N_{don}^+}{N_{don}} = 1 - \frac{b}{1 + g e^{-(E_{F_n} + E_{dop} - E_c)/kT}}, \tag{5a}$$

$$\frac{N_{acc}^-}{N_{acc}} = 1 - \frac{b}{1 + g e^{-(E_{dop} - E_{F_p} + E_v)/kT}}, \tag{5b}$$

where the function $b = b(N_{dop})$ describes the decreasing fraction of the bound states according to Eq. (4) and E_{dop} is the screening-dependent binding energy of the dopant. These equations contain the quasi-Fermi levels E_{F_n} and E_{F_p}. It is important to note that ii shifts the Fermi levels towards midgap, as is shown in the case of Si:P in Fig. 4. When using Eqs. (5a) and (5b) in a device simulator, the Fermi levels adjust themselves to their "real" (i.e., with ii) values due to the self-consistent solution of Poisson and continuity equations. The parameters of the simplified models (5a) and (5b) are listed in Table III. The deviations from the original models (1)–(4) are minor compared to the scattering of the experimental data in Figs. 1 and 3 and in Fig. 5 of Part I.

TABLE III. The parameters used to calculate the amount of incomplete ionization in device simulations.

Parameter	Si:P	Si:As	Si:B
$E_{dop,0}$ (meV)	45.5	53.7	44.39
N_{ref} (cm^{-3})	2.2×10^{18}	3×10^{18}	1.3×10^{18}
c	2	1.5	1.4
N_b (cm^{-3})	6×10^{18}	9×10^{18}	4.5×10^{18}
d	2.3	1.8	2.4
g	1/2	1/2	1/4

As discussed in Sec. IV, depletion or accumulation of free carriers may influence E_{dop}. In order to take such effects into account, E_{dop} and b should be taken as a function of $n + p$ instead of N_{dop}. This would not affect the results in neutral regions, where $n + p = N_{dop}$, but would improve the situation in space charge regions. We will discuss this point below.

For a device model it is advantageous to replace the Fermi levels in (5a) and (5b) by the densities. This is easily done in the case of Boltzmann statistics and leads to

$$\frac{N_{don}^+}{N_{don}} = 1 - \frac{bn}{n + g n_1}, \tag{6a}$$

$$\frac{N_{acc}^-}{N_{acc}} = 1 - \frac{bp}{p + g p_1}, \tag{6b}$$

with

$$n_1 = N_c e^{-E_{dop}/kT}, \quad p_1 = N_v e^{-E_{dop}/kT}. \tag{7}$$

It is interesting to note that for low doping densities (limit $E_{dop,0}$) the densities n_1 and p_1 take the values 2.35×10^{18}, 1.71×10^{18}, and 1.38×10^{18} cm^{-3} for phosphorus, arsenic, and boron, respectively, which are very close to the parameter N_{ref} in Table III. The difference between (5a) and (5b) and (6a) and (6b) is not larger than 1% and is only visible in the minima of the ionization level. This proves that using Boltzmann statistics in replacing Fermi levels by densities is indeed sufficient, because the ionization level quickly tends to 1 as the carriers become degenerate. Therefore, the maximum error occurs at the Mott density, where Boltzmann statistics is still a reasonable approximation.

Our recommended device model for ii is given by Eqs. (6a) and (6b) with dopant-density dependent functions b, [Eq. (4)] and E_{dop} [Eq. (2)] together with the parameters given in Table III. In order to demonstrate the effect of ii on device performance, we intended to implement this model into the device simulator DESSIS-ISE (Ref. 59) via the physical model interface (PMI). The PMI allows us to use our own models, however, within the restrictions of predefined dependencies in order not to jeopardize the robustness of the code. The most serious restrictions apply to the dependence on the carrier densities. In case of ii the predefined functionality in DESSIS-ISE is given by

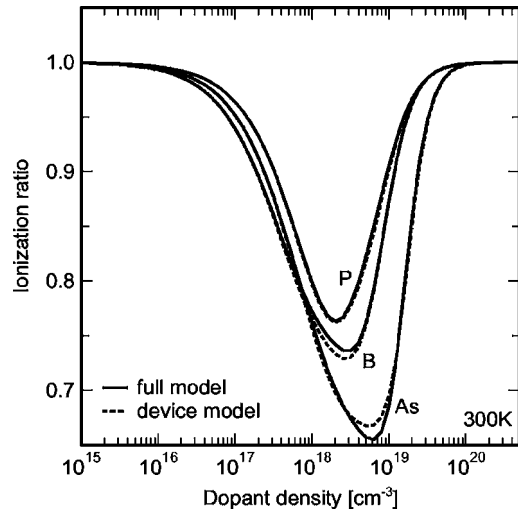$$\frac{N_{don}^+}{N_{don}} = \frac{1}{1 + g_D n/n_1}, \tag{8a}$$

FIG. 5. Ionization level for P, B, and As using the original model [Eqs. (1)–(4) (dashed line] and the approximated device model [Eqs. (8a) and (8b) with (10a) and (10b) (solid line].

$$\frac{N_{\mathrm{acc}}^-}{N_{\mathrm{acc}}} = \frac{1}{1 + g_A p/p_1}, \tag{8b}$$

where the "degeneracy factors" g_D and g_A can be modeled as function of temperature and doping, but not as function of the free carrier densities. When we transform our ii models (6a) and (6b) into the forms (8a) and (8b), we obtain the "effective degeneracy factors,"

$$g_D(T, N_{\mathrm{don}}, n, p) = \frac{b}{g + (1-b)n/n_1}, \tag{9a}$$

$$g_A(T, N_{\mathrm{acc}}, n, p) = \frac{b}{g + (1-b)p/p_1}. \tag{9b}$$

Besides their explicit dependence on the densities $n(p)$, an additional implicit dependence is given if the screening effect on the binding energies in the functions n_1 and p_1 is expressed by $n+p$. Replacing the densities by the ionized dopant concentration in (9a) and (9b) is only exact in neutral regions, but even then would make our ii model an implicit relation. For simplicity, we thus replace all densities in the effective degeneracy factors (9a) and (9b) by their respective total doping concentration,

$$g_D(T, N_{\mathrm{don}}) = \frac{b}{g + (1-b)N_{\mathrm{don}}/n_1}, \tag{10a}$$

$$g_A(T, N_{\mathrm{acc}}) = \frac{b}{g + (1-b)N_{\mathrm{acc}}/p_1}. \tag{10b}$$

The difference to the original model [Eqs. (1)–(4)] in neutral, uncompensated regions is shown in Fig. 5. Again, the deviations are minor compared to the scattering of the experimental data in Figs. 1 and 3 and in Fig. 5 of Part I. Note that for low doping concentration the effective degeneracy factors converge to the inverse g,

$$g_{D,A}(T, N_{\mathrm{dop}} \to 0) \to g^{-1}. \tag{11}$$

When using Eqs. (8a) and (8b) in a device simulator with constant $g_{D,A} = g^{-1}$ leads to an unphysical monotonous increase of ii with rising doping. Sometimes, as in DESSIS$_{\mathrm{-ISE}}$, a hard transition to complete ionization is enforced above N_{crit}. Our doping-dependent degeneracy factors (10a) and (10b) describe a smooth transition to complete ionization,

$$g_{D,A}(T, N_{\mathrm{dop}} \to \infty) \to 0, \tag{12}$$

based on the physical process that bound states gradually disappear in favor of extended states as the doping exceeds N_{crit}.

Replacing densities in the effective degeneracy factors (9a) and (9b) by the respective total doping concentration will cause a certain error in space charge regions. Inside depleted p-n junctions one should better replace them by zero in accord with the Schottky approximation. However, as is obvious from Eqs. (5a), (5b), (6a), (6b), (8a), and (8b), the degree of ionization becomes equal to 1 when the free carrier density vanishes. Therefore, the form of the effective degeneracy factors $g_{D,A}$ does not influence the degree of ionization as long as the distance between binding energy level and Fermi level is large compared to kT (and positive). The only slight error occurs at the boundaries of depletion regions. In the case of high injection, the excess carrier density strongly screens the Coulomb potential and would rather make the ionization complete (see the discussion in Sec. IV). However, a large error is not to be expected if the local carrier density takes the value of the injected density rather than that of the local ionized doping. This is indeed the case in important applications (see below).

VI. DEVICE EXAMPLES

We implemented the models (8a) and (8b) with (10a) and (10b) into the device simulator DESSIS$_{\mathrm{-ISE}}$ (Ref. 59) for the species P, As, and B. As first example, we simulate a double polyemitter n-p-n bipolar transistor of a 0.3 μm bipolar complementary metal-oxide-semiconductor (BiCMOS) process, where the geometry and doping information were taken from Ref. 60. The key points of this technology are the use of shallow and deep trench isolations to achieve a low collector-base junction capacitance and the use of a nonselective epitaxially grown base, aiming at high f_{max} and BV_{ceo}. Details of the dc and ac calibrations for this device can be found in Ref. 61. The simulated Gummel characteristics and the common-emitter current gain are depicted in Fig. 6 for the cases with and without ii, respectively. We observe an increase of the maximum gain by 25% due to the effect of incomplete ionization. This increase, which is related to the increase of the collector current at moderate V_{BE}, is directly caused by the lower active boron doping in the base, since the gain is proportional to $N_{\mathrm{don,emitter}}^+ / N_{\mathrm{acc,base}}^-$.

In the high-injection region, ii has the effect of a slightly faster saturation of the collector current. The rf transistor under study has a highly antimony-doped buried layer (with a peak concentration of 1.5×10^{19} cm^{-3}) to decrease the collector resistance. We used the phosphorus parameters of our model for antimony. The buried layer profile is a critical
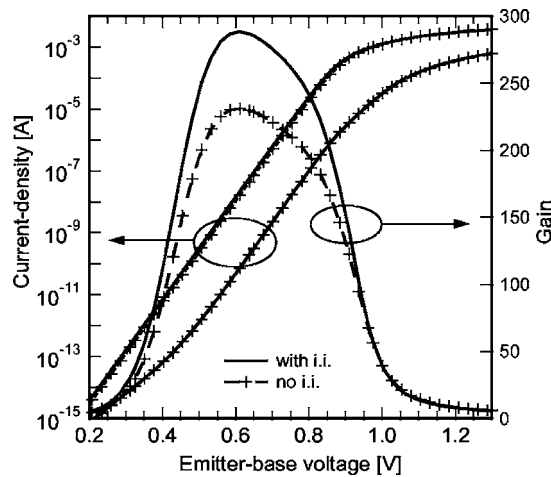
FIG. 6. Gummel characteristics and the gain of the double polyemitter *n-p-n* bipolar transistor.

issue and must be carefully modeled such that the soft breakdown in the early characteristics at high V_{CE} is best reproduced for all base currents. A stronger doping tail extending into the upper region of the collector causes an increase of the field strength and, consequently, enhances the avalanche multiplication. Furthermore, the collector doping profile affects the turn-on of the saturation current in the forward early characteristics, since a larger fraction of the collector bias can drop over the emitter-base junction at small V_{CE}. This shows that the ii model plays an important role in the modeling of the collector.

Figure 7 shows the density of ionized boron atoms (with and without the effect of ii) for different injection conditions. In the vicinity of the emitter-base junction the effect of ii disappears at small V_{BE} as discussed above. Increasing V_{BE} has the effect that the electron Fermi level approaches the boron binding energy level which results in an increased ii effect at the junction. In the high-injection range the density of the electron-hole plasma in the intrinsic base increases to far more than 10^{19} cm^{-3} and to more than 10^{18} cm^{-3} in the upper part of the collector. As can be seen from Eqs. (6a) and (6b), the ionization level becomes $1-b$ in the limit of very
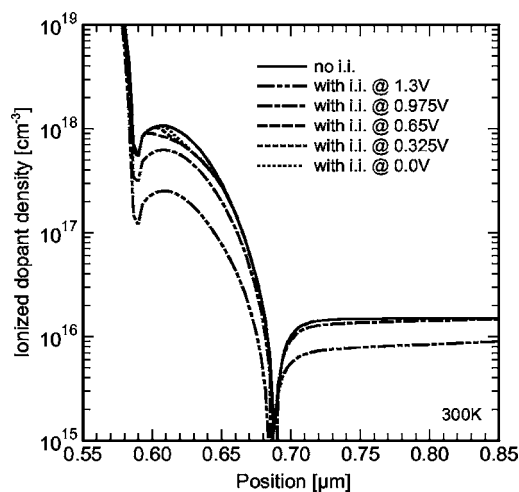
high injection, and ii artificially increases with decreasing ratio N_{dop}/N_b. Note that this artifact would not occur if b and E_{dop} could be modeled as function of the free carrier densities. Nevertheless, the artifact has no effect on the device behavior, because the injected carrier density is independent of the local ionized doping density in the high-injection region (the plasma density profiles with and without ii, respectively, are almost identical).

As second device example, we simulate crystalline Si thin-film solar cells, which are asymmetrical *p-n* diodes. Such cells are, in contrast to wafer cells, relatively highly doped in order to minimize resistive losses in lateral currents. To demonstrate the maximum possible impact of ii on the operation of such cells, we choose $N_{dop}=2\times10^{18}$ cm^{-3} in the boron-doped base, and phosphorus is diffused 1 μm deep into one surface to form a Gaussian emitter layer with a peak dopant density of 5×10^{18} cm^{-3}. The simulated open-circuit voltage V_{oc} decreases due to an ii from 624 to 614 mV, because the band-bending across the *p-n* junction is reduced. From the viewpoint of charge neutrality, the reduction of the hole majority carrier density increases the electron minority carrier density and hence the recombination rate in the base. In precise cell simulations, a reduction by 10 mV is a noticeable effect.

Besides the rf bipolar transistor and the thin-film solar cell, the impact of ii was studied for a number of other devices and phenomena: the transfer characteristics of a metal-oxide-semiconductor field-effect transistor (MOSFET), the *CV* characteristics of a MOS capacitor, and the gate direct tunnel current of a state-of-the-art MOSFET. In all examples, the active device regions had a doping concentration near the Mott density. Although ii had a visible effect in all cases, its size was found not to be of practical interest. In MOS devices, even with a boron substrate concentration of 2×10^{18} cm^{-3}, ii becomes negligible, since in the depletion region under the gate the effect of ii is not present (large distance between boron level and Fermi level), and in the inverted channel the carrier density is fixed by the amount of gate charge.

VII. CONCLUSIONS

The parametrization of the density of states (DOS) near the band edge of crystalline silicon was extended from phosphorus to arsenic and boron. The amount of incomplete ionization in Si:As is significantly larger than in Si:P, as expected from the differences in the energy of the dopant levels and in the Mott densities. The boron energy level has a distinctly different behavior as a function of dopant density than phosphorus. However, the amount of incomplete ionization is about the same in these two dopant types because the boron ground state is fourfold degenerate, while in phosphorus the degeneracy is twofold. A formula for incomplete ionization suitable for implementation in device simulators was derived. The simulations demonstrate that the current-gain of *p-n-p* bipolar transistors is increased by incomplete ionization by up to 25% and that the open-circuit voltage of thin-film silicon solar cells suffers by 10 mV.

FIG. 7. Profiles of the ionized doping density along a vertical cut through the *n-p-n* bipolar transistor for various emitter-base voltages.

[1] E. Abramof, A. Ferreira da Silva, B. E. Sernelius, J. P. de Souza, and H. Boudinov, Phys. Rev. B **55**, 9584 (1997).

[2] R. G. Aggarwal and A. K. Ramdas, Phys. Rev. **140**, A1246 (1965).

[3] D. Karaiskaj, T. A. Meyer, M. L. W. Thewalt, and M. Cordona, Phys. Rev. B **68**, 121201 (2003).

[4] A. Ferreira da Silva, J. Appl. Phys. **76**, 5249 (1994).

[5] T. F. Rosenbaum, R. F. Milligan, M. A. Paalanen, G. A. Thomas, R. N. Bhatt, and W. Lin, Phys. Rev. B **27**, 7509 (1983).

[6] A. Ferreira da Silva, Phys. Scr., T **T14**, 27 (1986).

[7] P. Newmann and D. F. Holcomb, Phys. Rev. B **28**, 638 (1983).

[8] D. W. Fischer and J. J. Rome, Phys. Rev. B **27**, 4826 (1983).

[9] P. Dai, Y. Zhang, and M. P. Sarachik, Phys. Rev. Lett. **66**, 1914 (1991).

[10] Y. Furukawa, J. Phys. Soc. Jpn. **16**, 577 (1961).

[11] F. J. Morin and J. P. Maita, Phys. Rev. **96**, 28 (1954).

[12] E. M. Omelyanovskii, V. I. Fistul, and M. G. Milvidskii, Sov. Phys. Solid State **5**, 676 (1963).

[13] G. A. Swartz, J. Phys. Chem. Solids **12**, 245 (1960).

[14] A. L. Lin, Appl. Phys. Lett. **53**, 776 (1988).

[15] P. E. Schmid, M. L. W. Thewalt, and W. P. Dumke, Solid State Commun. **38**, 1091 (1981).

[16] M. Migliuolo and T. G. Castner, Phys. Rev. B **38**, 11593 (1988).

[17] W. N. Shafarman, T. G. Castner, J. S. Brooks, K. P. Martin, and M. J. Naughton, Solid-State Electron. **28**, 93 (1985).

[18] G. Kaiblinger-Grujin, H. Kosina, and S. Selberherr, J. Appl. Phys. **83**, 3096 (1998).

[19] M. V. Fischetti and S. E. Laux, J. Appl. Phys. **85**, 7984 (1999).

[20] P. Altermatt, G. Heiser, and A. Schenk, J. Appl. Phys. **100**, 113714 (2006).

[21] R. A. Logan, J. F. Gilbert, and F. A. Trumbore, J. Appl. Phys. **32**, 131 (1961).

[22] H. I. Ralph, G. Simpson, and R. J. Elliott, Phys. Rev. B **11**, 2948 (1975).

[23] S. Solmi, M. Severi, R. Angelucci, L. Baldi, and R. Bilenchi, J. Electrochem. Soc. **129**, 1811 (1982).

[24] P. Newmann, M. J. Hirsch, and D. F. Holcomb, J. Appl. Phys. **58**, 3779 (1985).

[25] R. M. Swanson and S. E. Swirhun, Sandia National Laboratories Technical Report No. SAND97-7019.

[26] W. Scott and C. E. Jones, J. Appl. Phys. **50**, 7258 (1979).

[27] J. F. Lin, S. S. Li, L. C. Linares, and K. W. Teng, Solid-State Electron. **24**, 827 (1981).

[28] H. R. Chandrasekhar, P. Fisher, K. Ramdas, and S. Rodriguez, Phys. Rev. B **8**, 3836 (1973).

[29] D. Karaiskaj, M. L. W. Thewalt, T. Ruf, M. Cardona, and M. Konuma, Phys. Rev. Lett. **89**, 016401 (2002).

[30] T. H. Ning and C. T. Sah, Phys. Rev. B **4**, 3468 (1971).

[31] A. K. Ramdas and S. Rodriguez, Solid State Commun. **117**, 213 (2001).

[32] R. G. Pires, R. M. Dickstein, S. L. Titcomb, and R. L. Anderson, Cryogenics **30**, 1064 (1990).

[33] F. Fontaine, J. Appl. Phys. **85**, 1409 (1999).

[34] J. Wagner, Phys. Rev. B **32**, 1323 (1985).

[35] D. E. Cullen, E. L. Wolf, and W. Dale Compton, Phys. Rev. B **2**, 3157 1970.

[36] D. E. Cullen, Ph.D. thesis, University of Illionis, Urbana-Champaign, IL, (1970).

[37] G. Backenstoss, Phys. Rev. **108**, 1416 (1957).

[38] K. Wolfstirn, Phys. Chem. Solids **16**, 279 (1960).

[39] R. Baron, G. A. Shifrin, O. J. Marsh, and J. W. Mayer, J. Appl. Phys. **40**, 3702 (1969).

[40] M. E. Brinson and W. Dunstan, J. Phys. C **3**, 483 (1970).

[41] Y. Ochiai and E. Matsuura, Phys. Status Solidi A **27**, K89 (1975).

[42] R. E. Jones and B. Z. Li, J. Appl. Phys. **57**, 2802 (1985).

[43] H. J. Gossmann, F. C. Untetwald, and H. S. Luftman, J. Appl. Phys. **73**, 8237 (1993).

[44] T. Alzanki, R. Gwilliam, N. Emerson, and B. J. Sealy, Electron. Lett. **40**, 774 (2004).

[45] E. Abramof, A. Ferreira da Silva, B. E. Sernelius, J. P. de Souza, and H. Boudinov, J. Mater. Res. **12**, 641 (1997).

[46] M. Tajima, T. Masui, D. Itoh, and T. Nishino, J. Electrochem. Soc. **137**, 3544 (1990).

[47] G. Galvagno, A. La Ferla, F. La Via, V. Raineri, A. Gasparotto, A. Carnera, and E. Rimini, Semicond. Sci. Technol. **12**, 1433 (1997).

[48] L. C. Linares and S. S. Li, J. Electrochem. Soc. **128**, 601 (1981).

[49] Y. Sasaki, K. Itoh, E. Inoue, S. Kishi, and T. Mitsuishi, Solid-State Electron. **31**, 5 (1988).

[50] D. K. Schroder, T. T. Braggins, and H. M. Hobgood, J. Appl. Phys. **49**, 5256 (1978).

[51] J. Serre and A. Ghazali, Phys. Rev. B **28**, 4704 (1983).

[52] D. M. Luz, S. S. Makler, and E. V. Anda, J. Phys. C **21**, 5149 (1988).

[53] N. A. Penin, B. G. Zhurkin, and B. A. Volkov, Sov. Phys. Solid State **7**, 2580 (1966).

[54] Y. Nishio, K. Kajita, and W. Sasaki, Solid State Commun. **79**, 1017 (1991).

[55] U. Thomanschefsky and D. F. Holcomb, Phys. Rev. B **45**, 13356 (1992).

[56] M. J. Hirsch, D. F. Holcomb, R. N. Bhatt, and M. A. Paalanen, Phys. Rev. Lett. **68**, 1418 (1992).

[57] A. Ferreira da Silva, Phys. Rev. B **48**, 1921 (1993).

[58] M. Levy, P. Y. Yu, Y. Zhang, and M. P. Sarachik, Phys. Rev. B **49**, 1677 (1994).

[59] DESSIS, Version 10.0.6 Synopsys, Inc., Mountain View, CA, 2005.

[60] H. Nii *et al.*, IEEE Trans. Electron Devices **46**, 712 (1999).

[61] B. Schmithüsen, A. Schenk, I. Ruiz, and W. Fichtner, *Asian-Pacific Microwave Conference* (Allied Publishers Private Limited, New Delhi, India, 2004).